actuators

MDPI

Article

Implementation of an Active Ankle-Foot Orthosis Prototype with a Cam-Driven Actuator

Carlos Armando Lara-Velazquez [1], Juan-Pablo Ramirez-Paredes [1,*], Felipe J. Torres [2], Israel Martínez-Ramírez [2], Jeymar Baron-Casique [1], Diego A. Núñez-Altamirano [2] and Beatriz Verónica González-Sandoval [3]

[1] Department of Electronics Engineering, University of Guanajuato, Carretera Salamanca—Valle de Santiago km 3.5 + 1.8, Comunidad de Palo Blanco, Salamanca 36787, Mexico; ca.laravelazquez@ugto.mx (C.A.L.-V.); j.baroncasique@ugto.mx (J.B.-C.)

[2] Department of Mechanical Engineering, University of Guanajuato, Carretera Salamanca—Valle de Santiago km 3.5 + 1.8, Comunidad de Palo Blanco, Salamanca 36787, Mexico; fdj.torres@ugto.mx (F.J.T.); israel.martinez@ugto.mx (I.M.-R.); da.nunez@ugto.mx (D.A.N.-A.)

[3] Department of Medicine and Nutrition, University of Guanajuato, Blvd. Milenio 1001, Predio San Carlos, León de los Aldama 37670, Mexico; bvgonzalez@ugto.mx

* Correspondence: jpi.ramirez@ugto.mx; Tel.: +52-464-647-9940

Abstract: The high prevalence of conditions leading to foot drop highlights the need for devices that restore functionality, enabling patients to regain a natural gait pattern. There is a demand for a portable, lightweight, low-cost, and efficient active ankle-foot orthosis. In this work, we present the prototype of a new design that was simulated in a previous contribution, with a test bench evaluation of the low-level control. The dynamical behavior of a cam suspension interaction with a proportional–integral–derivative controller system for transmission is evaluated. The proposed active orthosis includes a novel cam-based actuator, designed to intervene at the dorsiflexion stage of gait, without influencing the plantar flexion. This design is aimed at specific lower limb ailments that cause a need for assistance only in raising the foot, and it leverages a commercial servomotor to achieve ankle angle tracking. System identification was performed using a test bench, with three degrees of freedom to emulate tibial motion during gait. Response evaluations of the device showed low values for the integral time squared error, peak overshoot, and settling time for step inputs, with and without additional periodic perturbations. The root mean squared error of the device while tracking an ankle angle signal varied from 0.1 to 6.5 degrees, depending on the speed of the changes.

Keywords: assistive devices; orthosis and prosthesis; control optimization

check for updates

Academic Editors: Monica Malvezzi, Monica Tiboni and Maria Cristina Valigi

Received: 17 October 2024
Revised: 7 January 2025
Accepted: 7 January 2025
Published: 5 February 2025

Citation: Lara-Velazquez, C.A.; Ramirez-Paredes, J.-P.; Torres, F.J.; Martínez-Ramírez, I.; Baron-Casique, J.; Núñez-Altamirano, D.A.; González-Sandoval, B.V. Implementation of an Active Ankle-Foot Orthosis Prototype with a Cam-Driven Actuator. *Actuators* **2025**, *14*, 72. https://doi.org/10.3390/act14020072

Copyright: © 2025 by the authors. Licensee MDPI, Basel, Switzerland. This article is an open access article distributed under the terms and conditions of the Creative Commons Attribution (CC BY) license (https://creativecommons.org/licenses/by/4.0/).

1. Introduction

Foot drop, a gait-altering condition characterized by the foot slapping down during each step, presents significant challenges for affected individuals. This condition, primarily caused by weakened foot and ankle dorsiflexor muscles, increases the risk of falls and injuries [1]. A recent study by Nath et al. [2] conducted a comprehensive retrospective analysis of foot-drop cases, identifying twenty-one potential causes. Notably, lumbosacral spine surgery emerged as the most frequent cause, accounting for 13.9% of cases. This high prevalence underscores the urgent need for reliable, affordable, portable, and comfortable assistive solutions, such as ankle-foot orthoses (AFOs) and exoskeletons.

Recent research has made significant strides in developing mechanical designs for AFOs. A comprehensive analysis by Lora-Milan et al. [3] examined various device cat-

egories, including passive, semi-active, and active orthoses. Their review encompassed devices featuring rigid transmissions, series elastic actuators (SEAs), cable-driven actuation, and pneumatic artificial muscles (PAMs). The study evaluated these technologies based on both laboratory testing and human trials, assessing their impacts on the gait kinematics, muscle activity, and energy expenditure. Among the evaluated technologies, SEAs demonstrated exceptional performance across most evaluation criteria.

Over the past two decades, researchers have explored various technological approaches to address foot drop, including functional electrical stimulation (FES) [4–6], active ankle-foot orthoses (AAFOs) [7–9], and hybrid systems combining multiple technologies. For instance, Hodgins et al. [10] developed an innovative control system integrating FES with PAMs. While their hybrid FES/PAM system showed improved performance, maintaining approximately 85% tracking accuracy after 60 cycles, compared to 45% for standalone FES, it faced limitations due to its tethered design and reliance on external compression systems. Researchers have made notable progress in developing compact pneumatic systems to enhance portability. Kim et al. [11] introduced a miniature compressor design that utilizes air's natural compliance for safe user interaction. However, this system's considerable weight of 2.6 kg and actuation delay limitations highlight ongoing challenges in the field.

Alternative approaches to ankle actuation have also been explored. For example, DeBoer et al. [12] introduced a novel, power-efficient actuator for an AAFO, based on a new principle of discrete non-linear stiffness combined with a crank-rocker configuration. In terms of control strategies, Jradi et al. proposed an adaptive active disturbance rejection controller (AADRC) [13], while Moon et al. developed a hybrid half-Gaussian selectively adaptive fuzzy control method. The latter was implemented in the AJ-1000 orthosis from Angel Robotics (South Korea) to reduce the control energy requirements [14]. These actuator and control system designs primarily aim to minimize the peak mechanical power and average motor energy consumption. However, they often do not prioritize reducing the device cost or weight. Many of these developments are tailored for drop foot treatment, with a review of such designs provided by Al-Rahmani et al. [15].

Some AAFO control strategies rely on position or speed controllers with significant damping, simplifying the control [16]. Certain models use bulky SEA devices to provide plantar flexion assistance [7]. Semi-active orthoses often utilize magneto-rheological (MR) fluids—smart materials whose rheological properties, such as viscosity, can be rapidly adjusted by applying a magnetic field. Chen et al. combined these two technologies in their robotic ankle-foot orthosis [17]. Recent efforts have focused on developing lightweight, adaptable AAFOs. Moltedo et al. [18] presented a spindle-driven system weighing 1.7 kg, while Yeung et al. [19] developed a rigid structure design prioritizing weight reduction. These developments, though promising, often involve trade-offs between weight, functionality, and adaptability. The implementation of control strategies requires thorough evaluation before human testing. The review by Baud et al. [16] proposed a three-layer classification framework for control strategies, emphasizing that rigid position control, typically implemented through proportional-integral-derivative (PID) regulators, remains the standard approach. However, systems with flexible components or variable environments often render high-precision positioning unnecessary and impractical. Control evaluations can be a repetitive and risky task to be performed directly with patients, so various research groups have developed test benches to evaluate their orthoses. For instance, Bedard et al. [20] built a test bench to evaluate a new ankle-foot orthosis (AFO) material composed of a carbon-infused polypropylene pre-impregnated fiber composite. Another example of a test bench is that of Maggioni et al. [21], featuring a bio-inspired model of a human leg, implemented on the leg orthosis of a robotic gait trainer. Other improvements and

evaluations related to the mechanical and control design of exoskeletons have also been reported [22,23].

As described by Kirtas et al. [24], the performance of an AAFO largely depends on its hardware and software design. They identified three primary control design approaches: variable impedance, torque, and trajectory tracking systems. A notable feature of their design is the use of a single sensor to detect the starting point of a new cycle and determine the stride frequency, which they highlighted as an advantage. However, their control algorithm for perturbation rejection may present a limitation, as it does not account for interaction forces. Their work includes a comparison of their algorithm with a PID controller through three tests: step response, trajectory tracking, and stride frequency. Kirtas et al. noted that their AAFO, like many similar devices in the literature, is designed for a range of applications, including the treatment of drop foot, cerebral palsy, and multiple sclerosis. This broad scope necessitates a robust design. Their evaluation focused on disturbances occurring primarily during the stance phase. However, the actuator's stout composition results in a device weight of 1.8 kg.

Based on these precedents, we present an alternative hardware design aimed to assist unilateral drop foot patients with a lightweight, low-cost device, built around a commercial servomotor. Our proposal addressing foot drop cases focuses on assisting with dorsiflexion, while acknowledging that patients may retain their plantar flexion capabilities. Unlike prior hardware designs for AAFOs in the literature, the design presented in this work is specifically limited to dorsiflexion assistance. Based on a previous study by our group [25], this design incorporates a lightweight, compliant element that can be easily replaced. This approach leverages the benefits of SEA technology while enabling the use of smaller, more compact components. A key innovation of our design is the inclusion of a novel cam system, which allows users to perform dorsiflexion movements freely, without restricting the plantar flexion. To evaluate the prototype, we constructed a test bench to simulate tibial movement during the gait cycle. A discrete PID controller was developed and tested using the system identification of the orthosis on the test bench, providing a foundation for future enhancements in control strategies. We evaluated the controller's performance with the primary approach of ankle trajectory tracking. The proposed orthosis, designed specifically for untethered operation, achieves accurate ankle angle tracking, even under external perturbations. The system is compact and lightweight, with a total mass of less than 1 kg, while maintaining a total component cost below USD 3000, making it an accessible option for researchers and potentially for clinical applications.

2. Materials and Methods

This project builds on a prior study conducted by our team [25], in which we described and optimized a novel AAFO design through simulation, addressing both mid-level and low-level control strategies. In this article, we present the prototype based on this design, incorporating the necessary adjustments and conducting evaluations using a test bench to emulate the swing phase of the gait cycle.

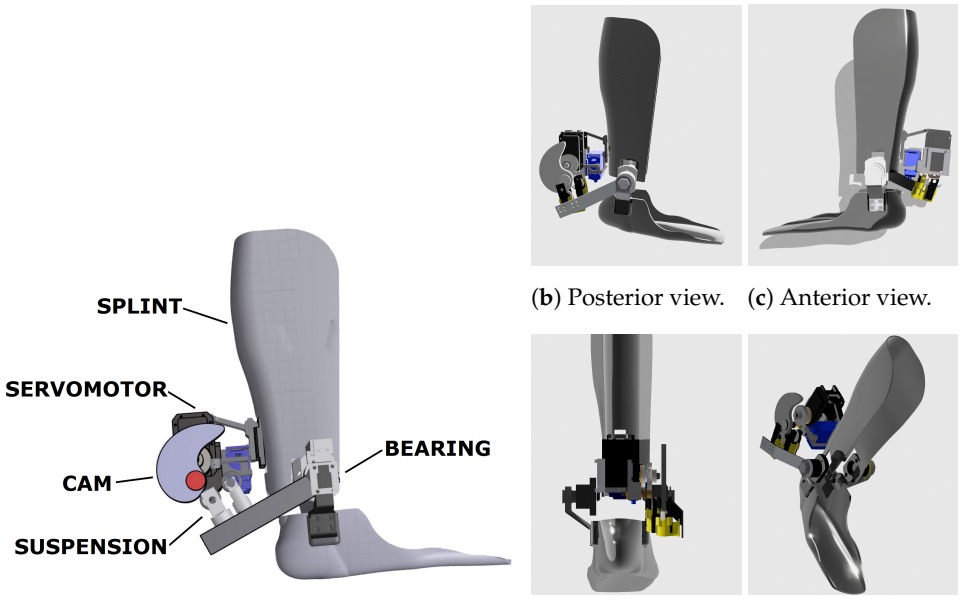
The current stage of prototype development, which precedes user evaluation, is critical in assessing material resistance, ensuring proper alignment, and identifying the range of operability. This stage is particularly important because the design aims to be not only reliable but also lightweight and cost-effective. Guided by the classification framework proposed by Baud et al. for exoskeleton control [16], this study focuses on the design and evaluation of the low-level control system.

After installing the prototype on the test bench, the actuation system underwent open-loop testing to assess its controllability and evaluate the performance of a discrete

PID controller. The following sections provide a brief description of the AAFO prototype, the test bench, and the proposed testing procedures.

2.1. AAFO Prototype Description

The actuation and transmission system of our AAFO assists dorsiflexion during the gait cycle using a cam suspension mechanism, while allowing free movement during plantar flexion. This design ensures that the user's movement is not overly restricted. Figure 1 depicts the CAD model of the prototype with its main components labeled.

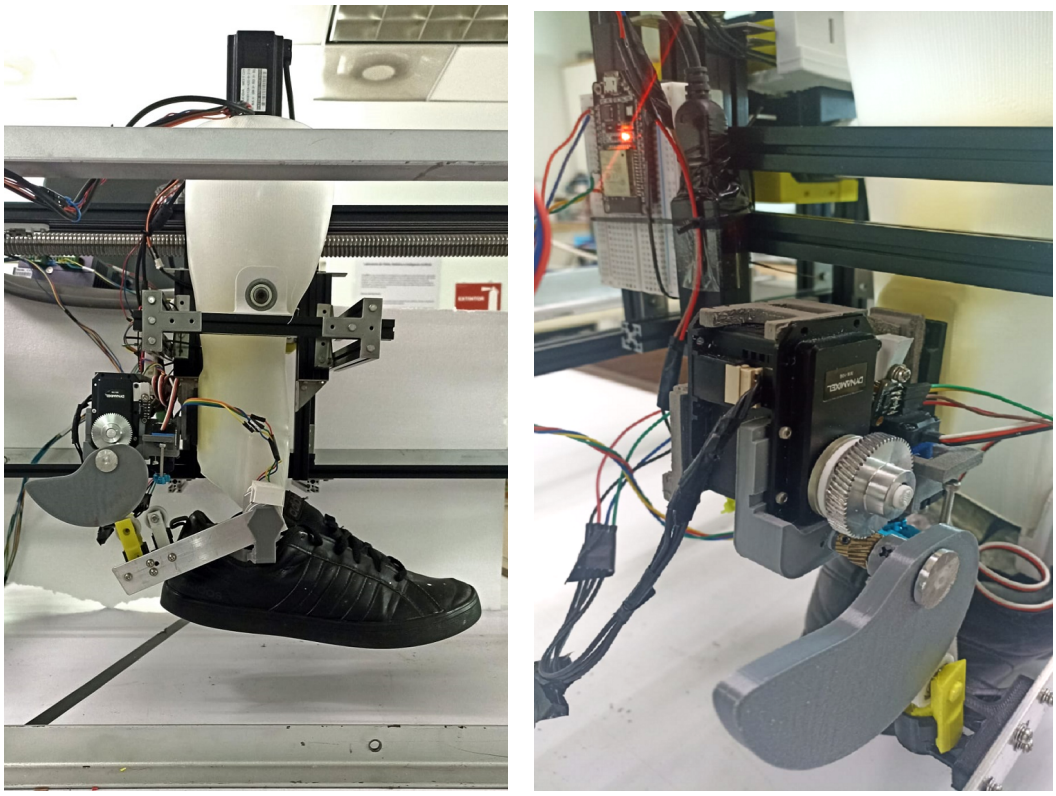


(**a**) Part names. (**b**) Posterior view. (**c**) Anterior view. (**d**) Rear view. (**e**) Isometric view.

Figure 1. CAD views of the prototype.

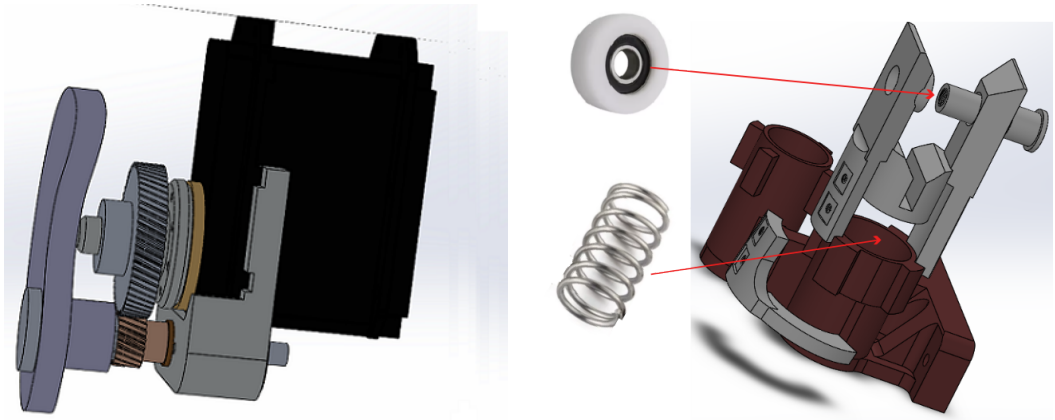
The cam transmits torque through contact with the wheels of a suspension system, which provides compliance. For the experiments in this work, we selected a spring with a high rigidity coefficient. The cam design features a radius change from 15 to 70 mm over 225 degrees, resulting in an ankle joint range of motion from 78 to 100 degrees. The MX-106 Dynamixel servomotor (ROBOTIS, Gangseo-gu, Republic of Korea) was configured in velocity mode with default, unmodified gains. We used an AS5600 rotary magnetic position sensor (ams-OSRAM AG, Premstaetten, Austria) to measure the ankle angles and a VL53L0X time-of-flight laser sensor (STMicroelectronics, Plan-les-Ouates, Switzerland) to control the cam's range of movement. The AAFO prototype, depicted in Figure 2, is constructed primarily from aluminum and plastic (ABS and Nylon with glass fibers) and weighs 1 kg, including the splint.

The transmission system features a cam linked to a gearbox connected to the servomotor's output (see Figure 3a). This cam transfers motion to the ankle by making contact with a special block, which incorporates a set of suspensions that serve as compliant elements to absorb shock. Figure 3b shows the suspension element design, which is in contact with the cam during the swing stage of the gait. The design is intended to simplify the process of replacing the compliant element (spring or damper). For this testing, a spring with a stiffness constant of 2.6 N/mm was used. In addition, a bearing is positioned and secured on each side of the ankle joint within the splint to ensure smooth single-axis motion.



(**a**) Frontal view. (**b**) Actuation–transmission view.

Figure 2. Orthosis prototype, assembled and mounted on test bench.



(**a**) Transmission design (**b**) Suspension element design

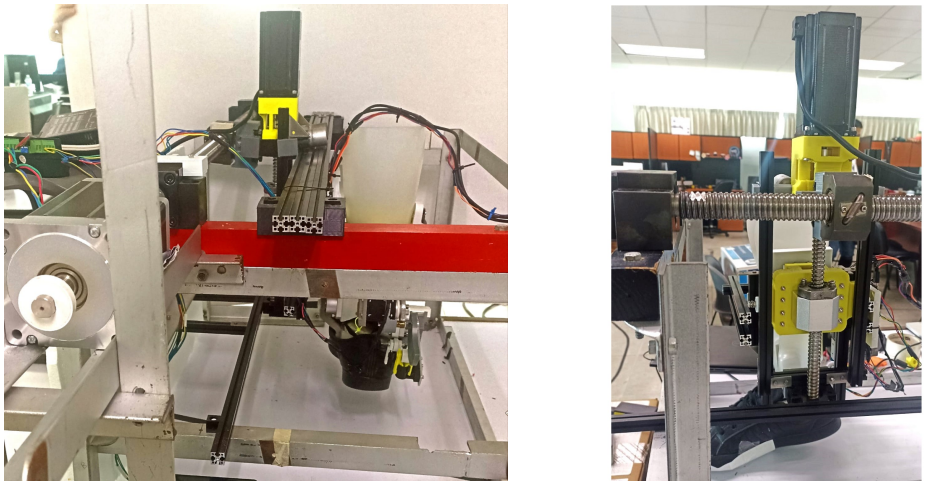
Figure 3. Detailed designs for the transmission and suspension elements.

2.2. Test Bench Description

A test bench was designed to evaluate the control system, allowing 3 degrees of freedom (DOF) to simulate tibial displacement and rotation during the gait cycle. Two lead screws, powered by stepper motors, control vertical (Z) and horizontal (X) movements, while a servomotor manages rotation. The rotation is applied near the tibia's center of mass. Reference tibial movements were obtained from markers recorded on healthy individuals during a typical gait cycle, sourced from the database presented in [26].

Tibial movement is controlled by an Arduino board, which simulates simultaneous 3-DOF movements. However, the system has limitations regarding the maximum displacement (90 cm) and velocity (12.5 mm/s), which are determined by the transmission system and stepper motor capabilities. The vertical and angular movement ranges of the test bench

were sufficient for this application, with a vertical range of 20 cm and an angular range of ±60 degrees. Figure 4 presents the transverse and rear views of the test bench.



(**a**) Transversal view. (**b**) Rear view.

Figure 4. Test bench views.

2.3. Control Design and Evaluation

The AAFO utilizes a PID controller for low-level control. The actuation–transmission system was evaluated by performing system identification with the orthosis mounted on the test bench. MATLAB's "System Identification" toolbox (R2020a) was used to develop a mathematical model to evaluate the controller gains, and the overall process is depicted in Figure 5.

The input signal used for identification was the sum of sinusoidal signals with different angular velocities, logarithmically spaced between 1 and 15 rad/s. Signal amplitudes of 3 and 5 were chosen for system identification and evaluation, respectively. An 8-variable state-space model was deemed most appropriate, achieving a match score above 80% between the actual and model-predicted responses. The system was subsequently tested for controllability, yielding positive results.

For the discrete control system, a backward Euler method was applied for both the integral and derivative terms. The transfer function for the discrete PID controller is described as follows:

$$C(z) = \frac{U(z)}{E(z)} = K_p + \frac{K_i T_s z}{z-1} + \frac{K_d N(z-1)}{(1+NT_s)z-1} \tag{1}$$

which can be rewritten in terms of negative powers of z as

$$\begin{aligned} C(z) = \alpha^{-1}[&(K_p(1+NT_s) + K_i T_s(1+NT_s) + K_d N) \\ &- (K_p(2+NT_s) + K_i T_s + 2K_d N)z^{-1} \\ &+ (K_p + K_d N)z^{-2}] \end{aligned} \tag{2}$$

where

$$\alpha = (1+NT_s) - (2+NT_s)z^{-1} + z^{-2} \tag{3}$$

and K_p, K_i, K_d are the proportional, integral, and derivative gains of the controller, respectively, N is the filter coefficient, and T_s is the sampling time. Finally, transforming the resulting expression to the time domain, we obtain the control function

$$u[k] = \frac{-(2+NT_s)}{1+NT_s}u[k-1] - \frac{1}{1+NT_s}u[k-2] + (K_p + K_iT_s + \frac{K_dN}{1+NT_s})e[k] + \\ + \frac{1}{1+NT_s}(K_p(2+NT_s) + K_iT_s + 2K_dN)e[k-1] + \frac{1}{1+NT_s}(K_p + K_dN)e[k-2]) \quad (4)$$

where $u[k]$ is the current control signal, and $u[k-1], u[k-2]$ represent the previous control signals. Similarly, $e[k]$ is the current error signal, with $e[k-1], e[k-2]$ representing previous error signals.

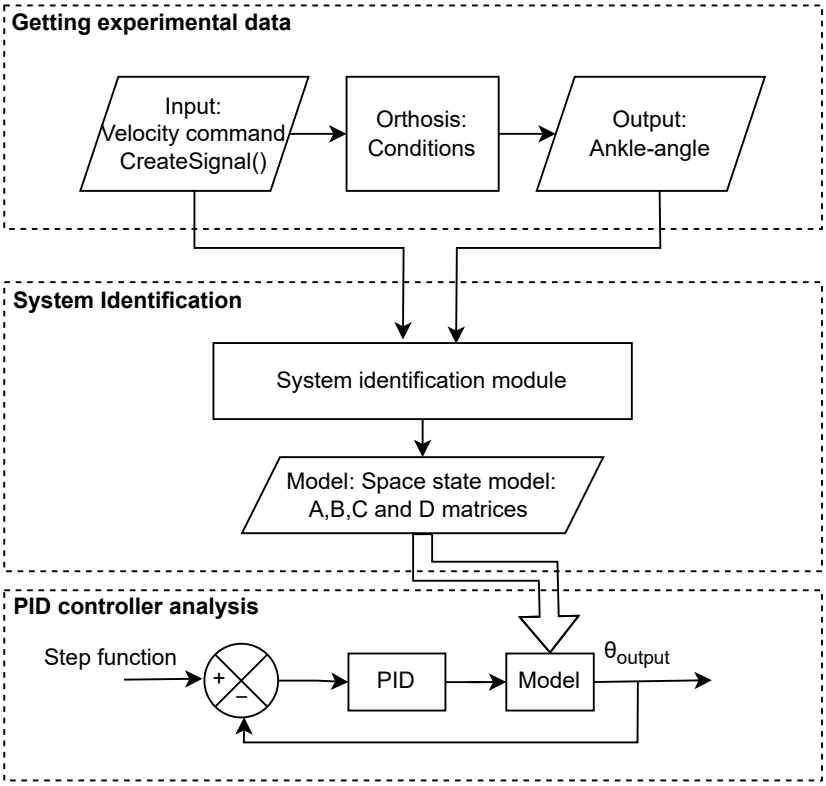


Figure 5. Overall process for system identification and PID controller synthesis.

After system identification, the discrete PID controller was evaluated in feedback mode. The stability was confirmed, as all poles of the system remained within the unit circle, with proportional, integral, and derivative gains of $K_p \leq 25$, $K_d \leq 5$, and $K_i \leq 5$, respectively.

To determine suitable PID parameters, we calculated the range of stability using the identified model. Brief optimization was performed based on this range and the physical constraints of the system, using the integral time squared error (ITSE) criterion as the loss function. A genetic algorithm was employed for optimization, with a population size of 100 and 150 generations. Guided by the range of stability found, the limits were set up as $K_p \in [0.1, 30]$, $K_i \in [0, 5]$, and $K_d \in [0, 5]$. The final optimized gains were $K_p = 22.527, K_i = 0.0011$, and $K_d = 2.727$, with a total cost of 0.7039. These values were used as a starting point for the fine-tuning of the real system, ultimately resulting in gains of 12.5, 0.4, and 0.6. A decreasing step signal from 103° to 94° was used to compare the real system's response with the model simulation, as shown in Figure 6.

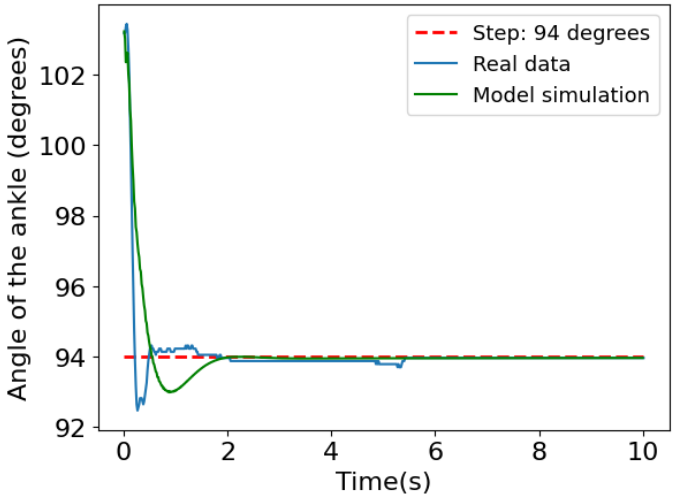


Figure 6. Step response for real vs. simulated AAFO, for a step input at 94 degrees.

2.4. Testing

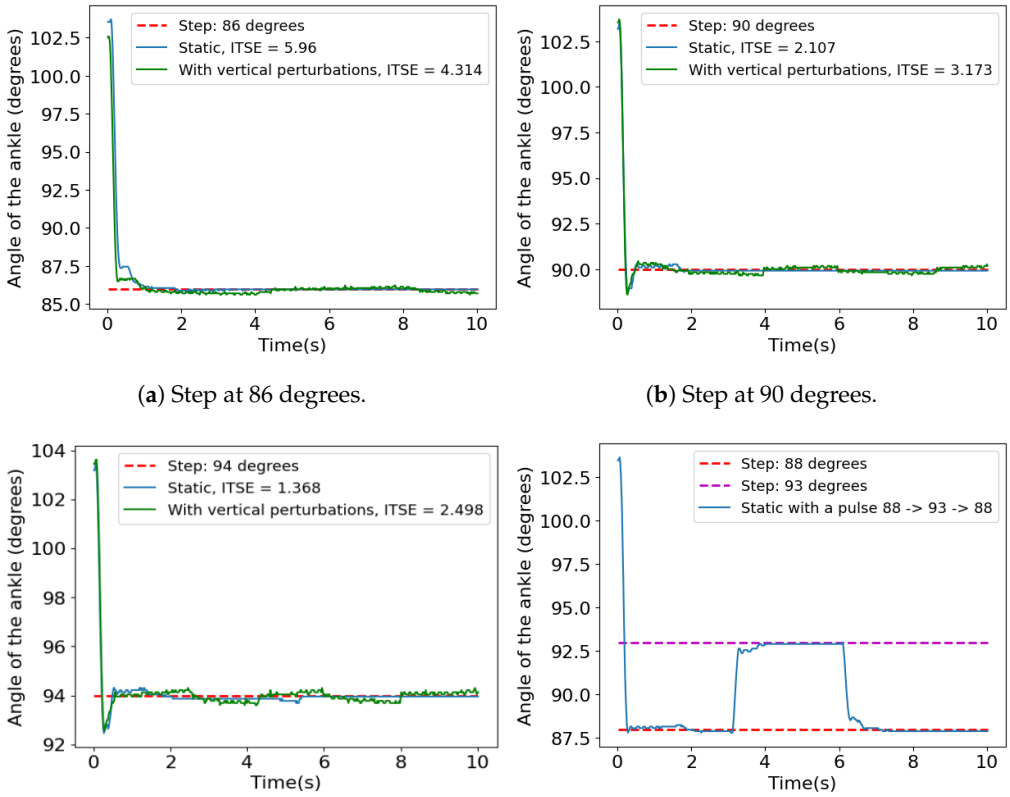
To evaluate the materials used in the prototype, the foot support was subjected to increasing loads, starting at 0.5 kg and progressing to 2 kg, while executing a basic routine following a reference signal. Additional tests were conducted with a 1.5 kg load. Two evaluations were performed to assess the step response control: a static test where only ankle movement was evaluated with the orthosis fixed and a second test involving vertical perturbations (5 mm displacement at 2 Hz). Both tests were conducted with reference signals of 86°, 90°, and 94°, starting from an initial angle of approximately 104°. The ITSE, peak overshoot, and settling time were measured for each test.

Additionally, a square impulse test was performed to evaluate sudden position changes. The reference signal was initially set to 88° from $t = 0$ to $t = 3$ s, after which a pulse of amplitude 5° was applied for three seconds, raising the signal to 93°, before returning to the baseline.

The next test was the response to tracking a gait cycle reference signal. In this case, we used one of the slower normal gait cycles reported by [26]. For this case, the response was evaluated for velocities scaled by a factor of 1/2, 1/4, 1/8, and 1/16 of the original signal to assess the system's accuracy at varying speeds. The mean squared error (MSE) was calculated for each case.

3. Results

Figure 7a, Figure 7b, Figure 7c illustrate the system's responses to 86°, 90°, and 94° step inputs, respectively. The red line represents the step reference, the blue line shows the static response, and the green line indicates the response under vertical perturbation. Figure 7d shows the system's response to a square pulse with an amplitude of 5°. The ITSE values were similar in both static and perturbed conditions, while the peak overshoot remained under 1.6° for all cases. The settling times were consistently below 0.8 s, even for the 94° step, which involved a 18° change. For the square pulse test, the system took less than 0.2 s to respond to a 5 change in amplitude. Table 1 reports the ITSE, peak overshoot, and settling time values for each scenario. The step response tests indicate that the system performs well under both static and dynamic conditions.



(**a**) Step at 86 degrees.

(**b**) Step at 90 degrees.

(**c**) Step at 94 degrees.

(**d**) Pulse response (5 degrees).

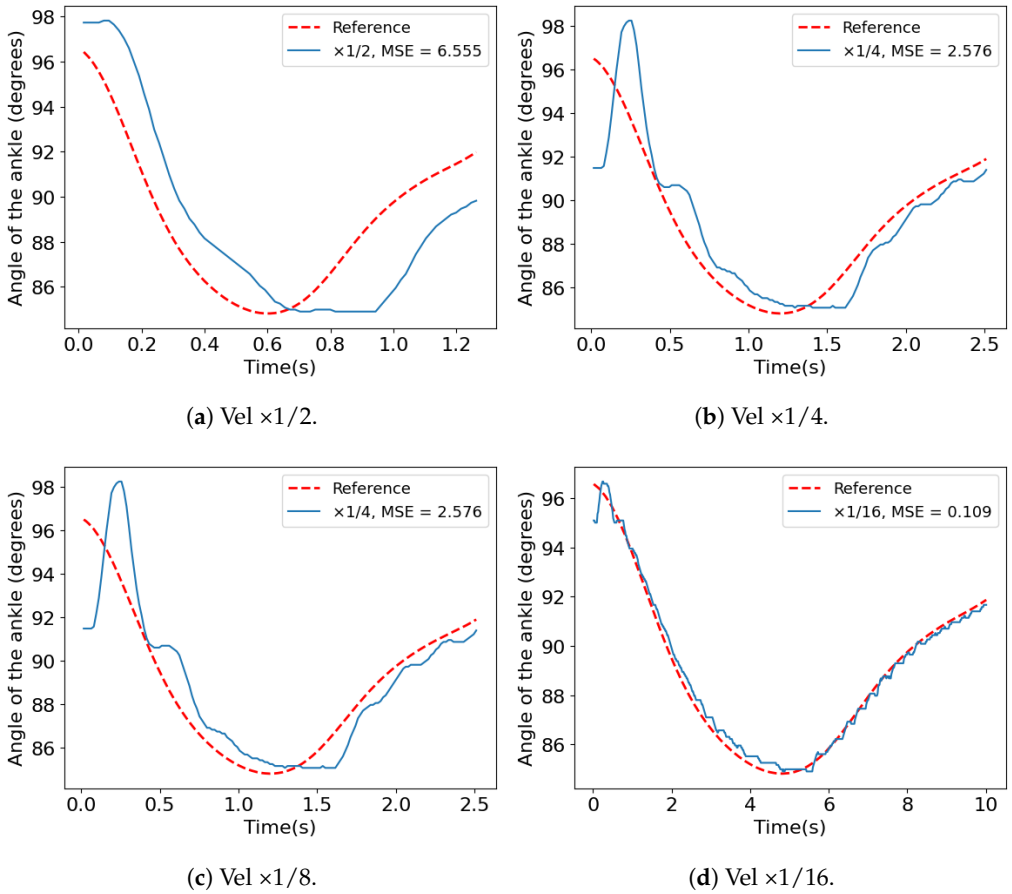
Figure 7. Step response of the AAFO prototype with and without vertical perturbations. The input steps are set to (**a**) 86 degrees, (**b**) 90 degrees, and (**c**) 94 degrees. (**d**) Pulse response, with base reference of 88 degrees and an added pulse of 5 degrees during 3 s.

Table 1. Evaluation of step response system with different step amplitudes and with and without vertical perturbation.

Test	ITSE	Peak Overshoot (°)	Settling Time (s)
86 static	5.96	-	0.703
90 static	2.107	1.231	0.431
94 static	1.368	1.539	0.463
86 with VP [1]	4.314	-	0.799
90 with VP [1]	3.173	1.406	0.384
94 with VP [1]	2.498	1.451	0.463

[1] VP: Vertical perturbations (shaking 5 mm up and down at 2 Hz).

The system's response to tracking the reference ankle position signal at varying speeds is depicted in Figure 8. The MSE values for each velocity are shown in the corresponding graphs, revealing that the error decreases as the velocity is reduced. Figure 8a demonstrates a nearly constant delay at half of the original velocity. At one-eighth (Figure 8c), the MSE drops to less than 1. The MSE decreases approximately 65-fold when comparing the maximum to the minimum velocity.



(**a**) Vel ×1/2. (**b**) Vel ×1/4.

(**c**) Vel ×1/8. (**d**) Vel ×1/16.

Figure 8. Tracking the reference ankle position signal with different velocities. Velocities are scaled by a factor of 1/2, 1/4, 1/8, and 1/16 with respect to the original.

4. Discussion

The prototype exhibited a functional range of motion, achieving 10° dorsiflexion and 10° plantar flexion from the neutral position. At 1 kg (excluding batteries), its weight represents a significant improvement over comparable devices, such as the 2.5 kg Pneumatic-AFO prototype developed by Ulkir et al. [27]. While both our work and the study by Ulkir's group employed different reference signals for the ankle angle during gait cycles, our PID control scheme demonstrated superior performance, with an RMS value of 0.2561, compared to their 0.5528. This performance metric is particularly noteworthy as it approaches the efficiency of their data-driven controller, underscoring the effectiveness of our meticulous PID gain tuning and system identification approach. The system's dynamic response characteristics, including a peak overshoot of 1.6° and rapid settling time, demonstrate robust performance for its intended application. Our velocity testing revealed an inverse relationship between the walking speed and tracking accuracy, with optimal performance achieved at one-eighth of the normal walking speed. This speed-dependent behavior suggests the need for further optimization to accommodate a broader spectrum of walking velocities in real-world applications. For future clinical trials, we propose incorporating ankle angle prediction algorithms, such as the finite state machine (FSM) described in [25], to enhance the system's responsiveness and adaptability.

Even at half the reference velocity, we observed tracking delays below 100 ms, outperforming systems such as that of Kim et al. [11], which exhibited inherent delays of a 130 ms rise time and 350 ms fall time. Our reference signal testing at approximately 1.8 km/h aligns with comparable studies in the field. For context, Kirtas et al. [24] conducted tracking performance assessments at 1.5, 2, and 2.5 km/h, all below typical walking speeds

(4.17 km/h for women and 4.32 km/h for men, as reported by Stolze et al. [28]). Similarly, the work by Kim et al. [11] utilized a gait frequency of 1 Hz (equivalent to about 3.6 km/h). Our comprehensive speed analysis revealed that increased walking speeds correlate with greater tracking delays. These delays, combined with potential splint deformations, could affect functionality through misalignment between the cam edges and the suspension block. Future research will expand to evaluate orthosis control across diverse walking patterns.

In terms of design objectives, our 1 kg prototype successfully balances functionality with portability. While some designs achieve lower weights, such as the 0.102 kg system by Hodgins et al. [10], they often sacrifice portability by requiring external components like air compressors. Our design achieves a weight comparable to the orthosis by Yeung et al. [19] while incorporating additional features, including reduced dorsiflexion rigidity and an integrated compliance element for actuator protection. These enhancements represent meaningful improvements in practical functionality without compromising the system's portability.

5. Conclusions

A novel active ankle-foot orthosis (AAFO) prototype was developed and evaluated. The cam suspension transmission system, combined with a PID controller, will provide swing phase assistance for individuals with foot drop. The low-level control system exhibited linear behavior, with an eight-variable state-space model identified as the most suitable representation. The results demonstrated that the system responded effectively to changes in the reference signal at walking speeds ranging from slow to normal.

This study successfully demonstrates the feasibility and potential of the developed AAFO prototype. With further refinement and user testing, the device could significantly enhance the mobility and quality of life of individuals with foot drop. The current hardware has the capacity for increased functionality by incorporating additional sensors, enabling the integration of mid-level and high-level control systems.

A limitation of the current prototype is the interaction between the cam and the suspension block, which requires the precise alignment of both components. The base splint, constructed from polypropylene, is susceptible to deformation under significant stress. Such deformation could induce misalignment, potentially affecting the device's performance. While misalignment did not occur during our tests, we anticipate that it could arise at higher gait speeds. This issue warrants further investigation before progressing to human trials.

Author Contributions: Conceptualization, C.A.L.-V. and J.-P.R.-P.; Methodology, J.-P.R.-P., F.J.T. and I.M.-R.; Software, C.A.L.-V. and J.B.-C.; Validation, J.B.-C.; Formal Analysis, J.-P.R.-P. and F.J.T.; Investigation, C.A.L.-V., I.M.-R. and D.A.N.-A.; Resources, J.-P.R.-P., F.J.T., I.M.-R., D.A.N.-A. and B.V.G.-S.; Data Curation, J.B.-C. and C.A.L.-V.; Writing—Original Draft, C.A.L.-V.; Writing—Review and Editing, J.-P.R.-P.; Visualization, C.A.L.-V.; Supervision, J.-P.R.-P. and B.V.G.-S.; Project Administration, J.-P.R.-P.; Funding Acquisition, J.-P.R.-P., B.V.G.-S. All authors have read and agreed to the published version of the manuscript.

Funding: This research was funded by the Innovation, Science and Entrepreneurship Institute for Competitiveness of Guanajuato State (IDEA GTO), under grant number IDEAGTO/CONV/033/2022. Author C.A.L.V. thanks the Mexican Council for Humanities, Science and Technology (CONAHCYT) for graduate fellowship 662285.

Institutional Review Board Statement: Not applicable.

Informed Consent Statement: Not applicable.

Data Availability Statement: The data presented in this study are available on request from the corresponding author.

Acknowledgments: We thank the Institute for Persons with Disabilities of Guanajuato State (INGUDIS) for their assistance in the construction of the prototype. Within INGUDIS, Ana E. Velázquez-Bustamante, Luis E. Pérez-Ramírez, and Ulises Juárez-López, from the Guanajuato State Center for Rehabilitation, led the collaboration with our institution for this project.

Conflicts of Interest: The authors declare no conflicts of interest. The funders had no role in the design of the study; in the collection, analyses, or interpretation of the data; in the writing of the manuscript; or in the decision to publish the results.

Abbreviations

The following abbreviations are used in this manuscript:

PID	Proportional–integral–derivative
AFO	Ankle-foot orthosis
AAFO	Active ankle-foot orthosis
SEA	Series elastic actuator
MR	Magnetorheological
FSM	Finite state machine
MSE	Mean squared error
PAM	Pneumatic artificial muscle
FES	Functional electrical stimulation
AADRC	Adaptive active disturbance rejection controller
ITSE	Integral time squared error

References

1. Stewart, J.D. Foot drop: Where, why and what to do? *Pract. Neurol.* **2008**, *8*, 158–169. [CrossRef] [PubMed]
2. Nath, R.K.; Somasundaram, C. Incidence, Etiology, and Risk Factors Associated with Foot Drop. *Eplasty* **2023**, *23*, e16. [PubMed]
3. Lora-millan, J.S.; Nabipour, M.; Asseldonk, E.V. Advances on mechanical designs for assistive ankle-foot orthoses. *Front. Bioeng. Biotechnol.* **2023**, *11*, 1188685. [CrossRef]
4. Alnajjar, F.; Zaier, R.; Khalid, S.; Gochoo, M. Trends and Technologies in Rehabilitation of Foot Drop: A Systematic Review. *Expert Rev. Med. Devices* **2021**, *18*, 31–46. [CrossRef] [PubMed]
5. Prenton, S.; Hollands, K.L.; Kenney, L.P. Functional electrical stimulation versus ankle foot orthoses for foot-drop: A meta-analysis of orthotic effects. *J. Rehabil. Med.* **2016**, *48*, 646–656. [CrossRef] [PubMed]
6. Sabut, S.K.; Bhattacharya, S.D.; Manjunatha, M. Functional Electrical Stimulation on Improving Foot Drop Gait in Poststroke Rehabilitation: A Review of its Technology and Clinical Efficacy. *Crit. Rev. Biomed. Eng.* **2013**, *41*, 149–160. [CrossRef] [PubMed]
7. Blaya, J.A.; Herr, H. Adaptive Control of a Variable-Impedance Ankle-Foot Orthosis to Assist Drop-Foot Gait. *IEEE Trans. Neural Syst. Rehabil. Eng.* **2004**, *12*, 24–31. [CrossRef] [PubMed]
8. Shorter, K.A.; Xia, J.; Hsiao-Wecksler, E.T.; Durfee, W.K.; Kogler, G.F. Technologies for Powered Ankle-Foot Orthotic Systems: Possibilities and Challenges. *IEEE/ASME Trans. Mechatron.* **2013**, *18*, 337–347. [CrossRef]
9. Ferris, D.P.; Czerniecki, J.M.; Hannaford, B. An ankle-foot orthosis powered by artificial pneumatic muscles. *J. Appl. Biomech.* **2005**, *21*, 189–197. [CrossRef] [PubMed]
10. Hodgins, L.; Freeman, C.T. A hybrid orthosis combining functional electrical stimulation and soft robotics for improved assistance of drop-foot. *Med. Eng. Phys.* **2023**, *115*, 103979. [CrossRef]
11. Kim, S.J.; Na, Y.; Lee, D.Y.; Chang, H.; Kim, J. Pneumatic AFO Powered by a Miniature Custom Compressor for Drop Foot Correction. *IEEE Trans. Neural Syst. Rehabil. Eng.* **2020**, *28*, 1781–1789. [CrossRef]
12. Deboer, B.; Hosseini, A.; Rossa, C. A Discrete Non-Linear Series Elastic Actuator for Active Ankle-Foot Orthoses. *IEEE Robot. Autom. Lett.* **2022**, *7*, 6211–6217. [CrossRef]
13. Jradi, R.; Rifai, H.; Mohammed, S. Adaptive Active Disturbance Rejection Control of an Actuated Ankle Foot Orthosis for Ankle Movement Assistance. *IEEE Robot. Autom. Lett.* **2024**, *9*, 367–374. [CrossRef]
14. Moon, H.; Maiti, R.; Sharma, K.D.; Amirat, Y.; Siarry, P.; Mohammed, S. Hybrid Half-Gaussian Selectively Adaptive Fuzzy Control of an Actuated Ankle–Foot Orthosis. *IEEE Robot. Autom. Lett.* **2022**, *7*, 9635–9642. [CrossRef]
15. Al-Rahmani, N.; Mohan, D.M.; Awad, M.I.; Wasti, S.A. Lower-Limb Robotic Assistance Devices for Drop Foot: A Review. *IEEE Access* **2022**, *10*, 51964–51994. [CrossRef]
16. Baud, R.; Manzoori, A.R.; Ijspeert, A.; Bouri, M. Review of control strategies for lower-limb exoskeletons to assist gait. *J. NeuroEng. Rehabil.* **2021**, *18*, 119. [CrossRef] [PubMed]

17. Chen, B.; Zi, B.; Wang, Z.; Li, Y.; Qian, J. Development of robotic ankle-foot orthosis with series elastic actuator and magneto-rheological brake. *J. Mech. Robot.* **2021**, *13*, 011002. [CrossRef]
18. Moltedo, M.; Bacek, T.; Junius, K.; Vanderborght, B.; Lefeber, D. Mechanical Design of a Lightweight Compliant and Adaptable Active Ankle Foot Orthosis. In Proceedings of the 2016 6th IEEE International Conference on Biomedical Robotics and Biomechatronics (BioRob), Singapore, 26–29 June 2016; pp. 1224–1229.
19. Yeung, L.F.; Ockenfeld, C.; Pang, M.K.; Wai, H.W.; Soo, O.Y.; Li, S.W.; Tong, K.Y. Randomized controlled trial of robot-assisted gait training with dorsiflexion assistance on chronic stroke patients wearing ankle-foot-orthosis. *J. NeuroEng. Rehabil.* **2018**, *15*, 51. [CrossRef] [PubMed]
20. Bedard, G.G.; Motylinski, J.; Call, B.; Gao, F.; Gray, L. Bench Test Validation of a Dynamic Posterior Leaf Spring Ankle-Foot Orthosis. *JPO J. Prosthetics Orthot.* **2015**, *28*, 30–37. [CrossRef]
21. Maggioni, S.; Stucki, S.; Lünenburger, L.; Riener, R.; Melendez-Calderon, A. A bio-inspired robotic test bench for repeatable and safe testing of rehabilitation robots. In Proceedings of the 2016 6th IEEE International Conference on Biomedical Robotics and Biomechatronics (BioRob), Singapore, 26–29 June 2016; pp. 894–899. [CrossRef]
22. Natali, C.D.; Toxiri, S.; Ioakeimidis, S.; Caldwell, D.G.; Ortiz, J. Systematic framework for performance evaluation of exoskeleton actuators. *Wearable Technol.* **2020**, *1*, e4. [CrossRef] [PubMed]
23. Schrade, S.O.; Menner, M.; Shirota, C.; Winiger, P.; Stutz, A.; Zeilinger, M.N.; Lambercy, O.; Gassert, R. Knee Compliance Reduces Peak Swing Phase Collision Forces in a Lower-Limb Exoskeleton Leg: A Test Bench Evaluation. *IEEE Trans. Biomed. Eng.* **2021**, *68*, 535–544. [CrossRef] [PubMed]
24. Kirtas, O.; Savas, Y.; Bayraker, M.; Baskaya, F.; Basturk, H.; Samur, E. Control Engineering Practice Design, implementation, and evaluation of a backstepping control algorithm for an active ankle–foot orthosis. *Control Eng. Pract.* **2021**, *106*, 104667. [CrossRef]
25. Lara-Velazquez, C.A.; Ramirez-Paredes, J.P.; González-Sandoval, B.V. Active Ankle–Foot Orthosis Design and Computer Simulation with Multi-Objective Parameter Optimization. *Appl. Sci.* **2024**, *14*, 2726. [CrossRef]
26. Schreiber, C.; Moissenet, F. A multimodal dataset of human gait at different walking speeds established on injury-free adult participants. *Sci. Data* **2019**, *6*, 111. [CrossRef] [PubMed]
27. Ulkir, O.; Akgun, G.; Nasab, A.; Kaplanoglu, E. Data-Driven Predictive Control of a Pneumatic Ankle Foot Orthosis. *Adv. Electr. Comput. Eng.* **2021**, *21*, 65–74. [CrossRef]
28. Stolze, H.; Kuhtz-buschbeck, J.P.; Mondwurf, C.; Boczek-Funcke, A.; Jo, K. Gait analysis during treadmill and overground locomotion in children and adults. *Electroencephalogr. Clin. Neurophysiol./Electromyogr. Mot. Control* **1997**, *105*, 490–497. [CrossRef] [PubMed]

Disclaimer/Publisher's Note: The statements, opinions and data contained in all publications are solely those of the individual author(s) and contributor(s) and not of MDPI and/or the editor(s). MDPI and/or the editor(s) disclaim responsibility for any injury to people or property resulting from any ideas, methods, instructions or products referred to in the content.